Biaxial torus around nematic point defects

S. Kralj,[1,2] E. G. Virga,[3] and S. Žumer[2,4]
[1]*Department of Physics, Faculty of Education, University of Maribor, Koroška 160, 2000 Maribor, Slovenia*
[2]*Institute Jožef Stefan, Jamova 39, 1000 Ljubljana, Slovenia*
[3]*Department of Mathematics, INFM Research Unit, University of Pavia, via Ferrata 1, 27100 Pavia, Italy*
[4]*Department of Physics, Faculty of Mathematics and Physics, University of Ljubljana, Jadranska 19, 1000 Ljubljana, Slovenia*
(Received 14 January 1999)

We study the biaxial structure of both line and point defects in a nematic liquid crystal confined within a capillary tube whose lateral boundary enforces homeotropic anchoring. According to Landau–de Gennes theory the local order in the material is described by a second-order tensor **Q**, which encompasses both uniaxial and biaxial states. Our study is both analytical and numerical. We show that the core of a line defect with topological charge $M=1$ is uniaxial in the axial direction. At the lateral boundary, the uniaxial ordering along the radial direction is reached in two qualitatively different ways, depending on the sign of the order parameter on the axis. The point defects with charge $M=\pm 1$ exhibit a uniaxial ring in the plane orthogonal to the cylinder axis. This ring is in turn surrounded by a torus on which the degree of biaxiality attains its maximum. The typical lengths that characterize the structure of these defects depend both on the cylinder radius and the biaxial correlation length. It seems that the core of the point defect does not depend on the far nematic director field in the bulk limit. [S1063-651X(99)07408-5]

PACS number(s): 61.30.Cz, 61.30.Jf

I. INTRODUCTION

Generally, in ordered media defects take different names in different contexts: so they are called dislocations, disclinations, singularities, or domain walls. The study of these defects is traditionally one of the most important fields of physics [1]. This is due to their presence in connection with diverse physical phenomena, where their contribution is crucial and often exhibits a universal behavior. They appear as a consequence of the universal concept of broken symmetry, either associated with a phase transition, or due to the topological characteristics of the confining boundary [2]. Defects in ordered media are singular regions exhibiting order parameter configurations that cannot be transformed into a homogeneous ground state via continuous transformations. In general, at a defect site some continuum field describing a defectless state of the system is not uniquely defined. The *core* of the singularity is indeed the region in space where a finer description of the states experienced by the system is needed to remedy such an apparent failure of the continuum theory: it mostly consists of a different phase with higher energy than the surrounding. The linear dimension of the core is roughly given by the correlation length of the relevant order parameter field employed to explore it.

In this respect, the majority of experiments were carried out in various liquid crystal phases [3]. This is because of the rich variety of qualitatively different defects exhibited by these fluids: they are reminiscent of singularities in other condensed media [1,4,5] and physical fields, such as cosmology [6,7], which are often less accessible experimentally. On the other hand, it is relatively easy and inexpensive to prepare adequate liquid crystal samples. The morphology of a defect can be controlled by choosing a suitable liquid crystal phase, a confining geometry, and a surface anchoring condition. On the micron length scale defect structures can easily be observed optically, due to the optical anisotropy of these molecules. Another advantage with liquid crystals is that they reach equilibrium structures on experimentally accessible time scales.

The nematic phase, on which we focus in this contribution, exhibits in general both point and line defects that are conventionally classified through their *topological charge M* (also called the *disclination index*) [1,4]. This is defined with respect to the surrounding nematic director field $\boldsymbol{n}$, which is singular exactly at the defect: around the defect the director rotates by the angle $2M\pi$. For point defects the *strength* $|M|$ is an integer, while for line defects it can also be half an integer, by the *head-tail* invariance of the nematic director.

The excess free energy associated with defects is in most cases roughly proportional to M^2 [8]. Consequently, defects with $|M|>1$ appear only rarely. Here, following the Landau–de Gennes theory, we employ a second-order tensor **Q** to describe the local molecular order: it encompasses within the same setting both uniaxial and biaxial states. A defect for $\boldsymbol{n}$ is generally not so for **Q**, and so **Q** is fit to explore the biaxial *structure* of the uniaxial defects.

There have been various studies devoted to the structure of both point and line defects in nematic liquid crystals; the following lists of references, though far from being exhaustive, witness the interest attracted, respectively, by these types of defects: [9–21], [2,10,21–23]. Nevertheless, despite this endeavor, several issues remained open. Among them are the detailed analysis of the biaxial structure of defects and the effects of confinement on their characteristic features. These questions have been answered only in part in [9,16,18,19,21,22]. Here we further explore the effect of cylindrical confinement on the biaxial structures of both line and point defects in uniaxial nematic liquid crystals.

The plan of the paper is the following. In Sec. II we introduce the mathematical model employed throughout the paper. In Sec. III we illustrate our main results, which are then discussed in the last section.

II. MODEL

A. Free energy

The local ordering of a nematic liquid crystal can be described by a tensor order parameter [16,24]:

$$\mathbf{Q}=\sum_{i=1}^{3} s_i \boldsymbol{e}_i\otimes\boldsymbol{e}_i\,, \tag{1}$$

where the orthogonal unit vectors $\boldsymbol{e}_i$ are clearly the eigenvectors of $\mathbf{Q}$, and s_i are the corresponding eigenvalues, that is, $\mathbf{Q}\boldsymbol{e}_i=s_i\boldsymbol{e}_i$. By Eq. (1), the tensor $\mathbf{Q}$ is symmetric because $\mathbf{Q}^T=\mathbf{Q}$; it is further required to be traceless:

$$\mathrm{tr}\,\mathbf{Q}=\sum_{i=1}^{3} s_i=0. \tag{2}$$

Consequently, $\mathbf{Q}$ is in general defined by five independent parameters. Three of them determine the orientation of the eigenvectors, and the remaining two the eigenvalues.

In the uniaxial ordering two eigenvalues are equal, and so only three independent parameters are needed to describe a nematic configuration. $\mathbf{Q}$ can then be given the form

$$\mathbf{Q}=s\left(\boldsymbol{n}\otimes\boldsymbol{n}-\frac{1}{3}\mathbf{I}\right), \tag{3}$$

where the scalar s is the uniaxial order parameter, and the unit vector $\boldsymbol{n}$ is the nematic director pointing along the local optic axis. In Eq. (3) s can have either sign: when it is positive the ensemble of molecules represented by $\mathbf{Q}$ tends to be aligned along $\boldsymbol{n}$, whereas when s is negative it tends to lie in the plane orthogonal to $\boldsymbol{n}$.

In practice, various perturbations can make a confined liquid crystal exhibit weakly biaxial states, especially in the vicinity of a defect for $\boldsymbol{n}$. Thus, the representation for $\mathbf{Q}$ in Eq. (3) is no longer valid throughout the region occupied by the material, and use has to be made of the complete representation in Eq. (1). In a real sample the state represented by $\mathbf{Q}$ changes from point to point, and so $\mathbf{Q}$ is to be regarded as a tensor field. Wherever $\mathbf{Q}=\mathbf{0}$, the nematic order is locally lost and the fluid becomes *isotropic*. A convenient quantity to measure the degree of biaxiality is the parameter β^2 defined by [25]

$$\beta^2=1-6\frac{(\mathrm{tr}\mathbf{Q}^3)^2}{(\mathrm{tr}\,\mathbf{Q}^2)^3}, \tag{4}$$

which ranges in the interval $[0,1]$. In all uniaxial states $\beta^2=0$, and a state with maximal biaxiality would correspond to $\beta^2=1$.

The free-energy density f of a nematic liquid crystal can be expressed as the sum of two terms:

$$f=f_e+f_b\,.$$

They are, respectively, the *elastic* and the *bulk* free-energy densities. The former depends on the distortion in space of the tensor field $\mathbf{Q}$; within a simplified model it can be given the form

$$f_e=L|\nabla\mathbf{Q}|^2, \tag{5}$$

where L is an elastic constant which does not depend on the temperature. This description corresponds to the approximation with equal Frank elastic constants for uniaxial nematics [26]. The bulk free-energy density f_b is a potential that promotes the uniaxial order in an undistorted nematic liquid crystal. It is conventionally described by an expansion in $\mathbf{Q}$ up to the fourth order [8]:

$$f_b=A(T-T_*)\mathrm{tr}\,\mathbf{Q}^2-B\,\mathrm{tr}\,\mathbf{Q}^3+C(\mathrm{tr}\,\mathbf{Q}^2)^2. \tag{6}$$

Here A, B, C are positive material constants, T is the temperature, and T_* is the nematic supercooling temperature. For $T>T_*$, the potential f_b attains a local minimum at the isotropic phase, whereas for $T<T_*$ this local minimum ceases to exist. The material constants in Eq. (6) are chosen so that the minimizer of f_b is a uniaxial order tensor like that in Eq. (3). Within this model the isotropic-nematic phase transition in the bulk occurs at the temperature $T_{IN}=T_*+B^2/24AC$. Moreover, the equilibrium value of the uniaxial scalar order parameter s_{eq} in Eq. (3) also depends on the temperature: $s_{\mathrm{eq}}(T):=s_0\{3+\sqrt{9-8[(T-T_*)/(T_{IN}-T_*)]}\}/4$, where $s_0:=s_{\mathrm{eq}}(T_{IN})=\sqrt{(3A/2C)(T_{IN}-T_*)}=B/4C$.

Here we will only be concerned with strong anchoring conditions, and so we need not consider any contribution to the free energy from the boundary.

B. Lyuksyutov constraint

In most cases the *I-N* phase transition is weakly first order, so reflecting relatively small values of the material constant B. Deep in the nematic phase B is approximately an order of magnitude smaller than both $A(T_*-T)$ and C. Thus, for weak elastic distortions a good approximation for both f and f_b is the following [27]:

$$f\approx f_b\approx A(T-T_*)\mathrm{tr}\,\mathbf{Q}^2+C(\mathrm{tr}\,\mathbf{Q}^2)^2.$$

This function attains its minimum for a value of $\mathrm{tr}\,\mathbf{Q}^2$ that can alternatively be expressed in terms of the equilibrium value of s within this approximation:

$$\mathrm{tr}\,\mathbf{Q}^2=\frac{A(T_*-T)}{2C}=\frac{2s_{\mathrm{eq}}^2}{3}. \tag{7}$$

In our model this is to be regarded as a constraint for $\mathbf{Q}$. Thus, we assume that the orientational order of a liquid crystal responds to local distortions in a way that leaves $\mathrm{tr}\,\mathbf{Q}^2$ unchanged, even for strong distortions. Two facts concerning this constraint are worth noting.

(i) Within this approximation the liquid crystal cannot melt locally and become isotropic, because $\mathbf{Q}$ cannot vanish. From a physical point of view, this *scenario* is plausible in the deep nematic phase, where melting becomes exceedingly costly.

(ii) In Eq. (6) only the cubic term makes the uniaxial states preferred to the biaxial ones. Thus, we will keep this term in as a perturbation to the free-energy density on the states that minimize the leading terms in f_b.

Henceforth we take the constraint in Eq. (7) as valid. Consequently, only one parameter is needed to determine all eigenvalues of $\mathbf{Q}$.

C. Parametrization

We study a nematic liquid crystal confined within an infinite cylindrical cavity with radius R. The cylindrical coordinates are represented by $\{r,\vartheta,z\}$, and the corresponding unit vectors along the coordinate axes are $\boldsymbol{e}_r$, $\boldsymbol{e}_\vartheta$, and $\boldsymbol{e}_z$. We confine attention to distortions where the eigenvectors of $\mathbf{Q}$ can be expressed as

$$\boldsymbol{e}_1=\cos\varphi\,\boldsymbol{e}_r+\sin\varphi\,\boldsymbol{e}_z,\quad \boldsymbol{e}_2=-\sin\varphi\,\boldsymbol{e}_r+\cos\varphi\,\boldsymbol{e}_z,\quad \boldsymbol{e}_3=\boldsymbol{e}_\vartheta, \tag{8}$$

where φ is an angle ranging in the whole real axis. Thus, in going from a point within the cylinder to the next the eigenvectors of $\mathbf{Q}$ can only rotate around the $\boldsymbol{e}_\vartheta$ axis. This excludes, for example, any distortion twisted along the axis of the cylinder.

It is easily checked that both constraints Eqs. (2) and (7) are identically satisfied when the eigenvalues of $\mathbf{Q}$ are given the following representation in terms of a single angle ψ:

$$s_1=\frac{2}{3}s_{\rm eq}\cos\psi,\quad s_2=-\frac{2}{3}s_{\rm eq}\cos\left(\psi+\frac{\pi}{3}\right),$$

$$s_3=-\frac{2}{3}s_{\rm eq}\cos\left(\psi-\frac{\pi}{3}\right). \tag{9}$$

Moreover, the degree of biaxiality defined in Eq. (4) can be expressed as a function of ψ:

$$\beta^2=1-16\cos^2\psi\cos^2\left(\psi-\frac{\pi}{3}\right)\cos^2\left(\psi+\frac{\pi}{3}\right), \tag{10}$$

which is periodic with period $\pi/3$. For $i\in\{1,2,3\}$, the configurations with $\psi=(i-1)2\pi/3-\pi$ correspond to uniaxial states with negative order parameter and nematic director along $\boldsymbol{e}_i$, while the configurations with $\psi=(i-1)2\pi/3$ correspond to uniaxial states with opposite order parameter, but respectively the same director. It easily follows from Eq. (10) that these are the only zeros of β^2 in $[-\pi,\pi]$. The states with other values of ψ reflect biaxial molecular distributions. The degree of biaxiality attains its maximum for $\psi=(j-1)\pi/6$, $j\in\{1,\ldots,6\}$. The essential features of this representation for $\mathbf{Q}$ are illustrated in Fig. 1.

Through Eqs. (8) and (9) we describe all biaxial structures admissible in our model by use of only two parameters, namely, φ and ψ. The tensor $\mathbf{Q}$ delivered by Eq. (1) can then be regarded as a function of φ and ψ, which, however, is not injective. There are indeed transformations in the parameters φ and ψ that leave $\mathbf{Q}$ unchanged. Two of them are immediate consequences of the parametrization itself: they are embodied by the identities

$$\mathbf{Q}(\varphi,\psi)=\mathbf{Q}(\varphi,\psi+2k\pi),\quad \mathbf{Q}(\varphi,\psi)=\mathbf{Q}(\varphi+k\pi,\psi),$$

valid for all relative integers k. Changing ψ into $\psi+2k\pi$ or φ into $\varphi+k\pi$ does not affect $\mathbf{Q}$, because its eigenvalues remain the same and its eigenvectors just get reversed. Besides these trivial transformations, there is another which is not so, that is,

$$\{\varphi,\psi\}\to\left\{\varphi+\frac{\pi}{2},\frac{2\pi}{3}-\psi\right\}. \tag{11}$$

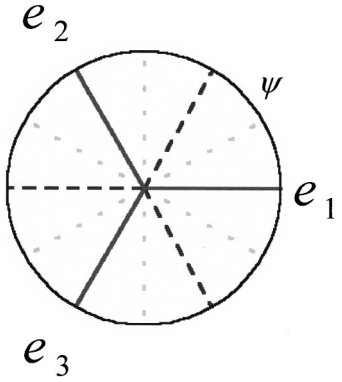

FIG. 1. The nematic states described by the order parameter ψ. Full lines: uniaxial states with a positive eigenvalue and nematic director along $\boldsymbol{e}_i$ ($i=1$, $\psi=0$; $i=2$, $\psi=2\pi/3$; $i=3$, $\psi=-2\pi/3$). Dashed lines: uniaxial states with a negative eigenvalue and nematic director along $\boldsymbol{e}_i$ ($i=1$, $\psi=\pi$; $i=2$, $\psi=-\pi/3$; $i=3$, $\psi=\pi/3$). Dotted lines: states with maximal degree of biaxiality.

This exchanges s_1 and s_2, maps $\boldsymbol{e}_1$ into $\boldsymbol{e}_2$, and $\boldsymbol{e}_2$ into $-\boldsymbol{e}_1$, while leaving both s_3 and $\boldsymbol{e}_3$ unchanged: by Eq. (1), it has no effect on $\mathbf{Q}$. The identity

$$\mathbf{Q}(\varphi,\psi)=\mathbf{Q}\left(\varphi+\frac{\pi}{2},\frac{2\pi}{3}-\psi\right)$$

will play a central role in the following. In particular, it ensures that both φ and ψ can suffer a jump without causing any discontinuity in $\mathbf{Q}$. We shall exploit this indeterminacy to represent a continuous field $\mathbf{Q}$ through discontinuous fields φ and ψ, whenever this does not cause a divergence in the free-energy functional.

D. Scaling

In the strong anchoring limit the only relevant characteristic length entering the model is the biaxial correlation length (see Appendix)

$$\xi_b:=\sqrt{\frac{2L}{3Bs_{\rm eq}}}. \tag{12}$$

It can easily be expressed in terms of the uniaxial correlation length $\xi_n:=\sqrt{L/A(T_{IN}-T_*)}$ at the I-N phase transition as

$$\xi_b=\frac{\xi_n}{3}\sqrt{\frac{s_{\rm eq}(T_{IN})}{s_{\rm eq}(T)}}. \tag{13}$$

For later use, we measure the free energy F in terms of $F_0:=RLs_{\rm eq}^2$ and the order parameter in terms of $s_0=s_{\rm eq}(T_{IN})$: thus, in the following $F\to F_0F$ and $s\to s_0s$. We further introduce the reduced temperature $\tau:=(T-T_*)/(T_{IN}-T_*)$ and measure all lengths relative to the cylinder radius R, so that $r\to Rr$, $z\to Rz$, $\xi_b\to R\xi_b$, $\xi_n\to R\xi_n$, $\boldsymbol{\nabla}\to(1/R)\boldsymbol{\nabla}$; in these units $R=1$, $s_{\rm eq}^2=-\frac{1}{2}\tau$. For convenience, we also define the *excess free energy* as $\Delta F:=F-F_{\rm bulk}$, where $F_{\rm bulk}$ denotes the free energy of a bulk-undistorted nematic.

In terms of these definitions one obtains the following dimensionless expression for the excess free energy of the nematic liquid crystal stored in a cylinder with length h:

$$\Delta F=\frac{16\pi}{3}\int_0^1 r\,dr\int_{-h/2}^{+h/2}dz\left(\frac{1}{\xi_b^2}\sigma_b+\sigma_e\right), \tag{14}$$

where

$$\sigma_b:=\frac{1}{18}(1-\cos 3\psi), \tag{15}$$

$$\sigma_e:=\frac{1}{4}|\nabla\psi|^2+\sin^2\left(\psi-\frac{\pi}{3}\right)|\nabla\varphi|^2 + \frac{\sin^2(\psi+\pi/3)\cos^2\varphi}{r^2}+\frac{\sin^2\psi\sin^2\varphi}{r^2}. \tag{16}$$

The corresponding Euler-Lagrange equations are

$$\nabla^2\psi-\frac{1}{\xi_b^2}\frac{\sin 3\psi}{3}-2\sin\left[2\left(\psi-\frac{\pi}{3}\right)\right]|\nabla\varphi|^2 + \frac{2\{\sin[2(\psi+\pi/3)]\cos^2\varphi+\sin 2\psi\sin^2\varphi\}}{r^2}=0, \tag{17}$$

and

$$\sin^2\left(\psi-\frac{\pi}{3}\right)\nabla^2\varphi+(\nabla\varphi\cdot\nabla\psi)\sin\left[2\left(\psi-\frac{\pi}{3}\right)\right] + \sin 2\varphi\,\frac{\sin^2(\psi+\pi/3)-\sin^2\psi}{2r^2}=0. \tag{18}$$

In these equations $\nabla\alpha=(\partial\alpha/\partial r)\boldsymbol{e}_r+(\partial\alpha/\partial z)\boldsymbol{e}_z$ and $\nabla^2\alpha=\partial^2\alpha/\partial r^2+(1/r)(\partial\alpha/\partial r)+\partial^2\alpha/\partial z^2$, for α either φ or ψ.

E. Boundary conditions

We assume that the lateral boundary of the cylinder enforces the strong homeotropic anchoring condition so that the nematic order is uniaxial along $\boldsymbol{e}_r$ with positive order parameter:

$$\mathbf{Q}|_{r=1}=\mathbf{Q}_{r+}:=s_{\rm eq}\left(\boldsymbol{e}_r\otimes\boldsymbol{e}_r-\frac{1}{3}\mathbf{I}\right). \tag{19}$$

This state can be described by the pair $\{\varphi,\psi\}=\{0,0\}$, which by Eq. (11) is completely equivalent to the pair $\{\pi/2,2\pi/3\}$.

It follows from Eq. (14) that for the integral to converge, only two pairs $\{\varphi,\psi\}$ are admissible on the cylinder axis, namely, $\{0,2\pi/3\}$ and $\{0,-\pi/3\}$. They correspond to the following tensors:

$$\mathbf{Q}_{z+}:=\mathbf{Q}(0,2\pi/3)=s_{\rm eq}\left(\boldsymbol{e}_z\otimes\boldsymbol{e}_z-\frac{1}{3}\mathbf{I}\right), \tag{20}$$

$$\mathbf{Q}_{z-}:=\mathbf{Q}(0,-\pi/3)=-\mathbf{Q}_{z+}, \tag{21}$$

which represent uniaxial states with nematic director along $\boldsymbol{e}_z$ and opposite scalar order parameters. Clearly, by Eq. (11) the same states are also represented by the pairs $\{\pi/2,0\}$ and $\{\pi/2,\pi\}$, respectively. Besides Eq. (19), $\mathbf{Q}$ will also be subject to either $\mathbf{Q}|_{r=0}=\mathbf{Q}_{z+}$ or $\mathbf{Q}|_{r=0}=\mathbf{Q}_{z-}$.

The equilibrium nematic structures subject to these boundary conditions were obtained numerically from the above Euler-Lagrange equations by using the over-relaxation method [28].

III. RESULTS

A. Line defects

We first restrict attention to distortions where $\mathbf{Q}$ only varies with the r coordinate. With the terminology introduced in [29], possible minimizers for this one-dimensional problem are the escaped radial structure (ER) and two qualitatively different planar radial solutions (PR) with either positive or negative scalar order parameter at $r=0$ (respectively, denoted by PR_+ and PR_-). In the genuinely uniaxial description, both PR structures would exhibit a line defect with strength 1 along the axis [1].

It is also expedient recalling the uniaxial ER structure [30] for the role it plays in our study of point defects. In this solution both boundary conditions $\mathbf{Q}_{z+}$ and $\mathbf{Q}_{r+}$ are met by simply rotating the eigenvectors of $\mathbf{Q}$ while r spans the interval $[0,1]$. In our setting, it is represented by the pair of functions $\{\varphi_{\rm ER},\psi_{\rm ER}\}$, where

$$\varphi_{\rm ER}(r):=\frac{\pi}{2}-2\arctan r,\qquad \psi_{\rm ER}\equiv 0. \tag{22}$$

The corresponding excess free energy is $\Delta F_{\rm ER}=8\pi h$ in dimensionless units.

On the contrary, in the PR solutions the eigenvectors remain fixed relative to the frame $\{\boldsymbol{e}_r,\boldsymbol{e}_\vartheta,\boldsymbol{e}_z\}$, so that $\varphi\equiv 0$ for both: the uniaxial states at $r=0$ and $r=1$ are connected through an *exchange* between the eigenvalues of $\mathbf{Q}$ [22]; here this is described as a change in the angle ψ, which starts from 0 at $r=1$ and reaches either $2\pi/3$ or $-\pi/3$ at $r=0$, in the solutions PR_+ and PR_-, respectively. We denote by $\psi_{\rm PR+}$ and $\psi_{\rm PR-}$ the functions of r that describe these solutions: their graphs are shown in Fig. 2(a).

While $\psi_{\rm PR-}$ ranges in the interval $[-\pi/3,0]$, thus crossing no uniaxial state for all $0<r<1$, $\psi_{\rm PR+}$ crosses at $r=r_{un}$ the uniaxial state with $\psi=\pi/3$, which has negative order parameter and nematic director along $\boldsymbol{e}_\vartheta$. Figure 2(b) illustrates the degree of biaxiality of both solutions for $R/\xi_b\sim 10$.

In the PR_+ solution the nematic ordering attains the maximal biaxiality at r_{b1} and r_{b2}, where $0<r_{b1}<r_{un}<r_{b2}<1$.

For the PR_- solution, however, there is a single value of r with maximal biaxiality; this will be denoted by r_b. The influence of the confinement on these parameters is shown in Fig. 3. For $R\gg\xi_b$ they all come close to $2\xi_b$, yielding the size of the defect core in the bulk.

When $R/\xi_b=0$ there are analytic expressions for both PR solutions. Although this limit is unphysical the solutions exhibit the general features recalled above. In this limit and for $\varphi=0$, the free energy in Eq. (14) reduces to

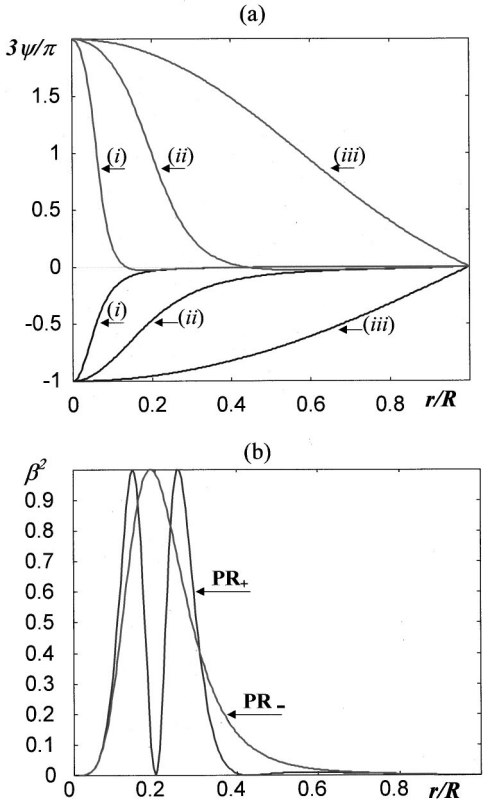

FIG. 2. Spatial structure of the PR_- and PR_+ solutions. (a) $\psi=\psi(r)$ for different values of R/ξ_b; $\varphi\equiv 0$. At $r=0$, $\psi=2\pi/3$ in the PR_+ solution and $\psi=-\pi/3$ in the PR_- solution. The curves labeled with (i), (ii), and (iii) correspond to $(R/\xi_b)^2=1350$, 135, and 0, respectively. (b) $\beta^2=\beta^2(r)$ for $(R/\xi_b)^2=135$.

$$\Delta F_{\mathrm{PR}}=\frac{16\pi h}{3}\int_0^1\left(\frac{1}{4}\chi'^2+\frac{\sin^2\chi}{r^2}\right)r\,dr, \tag{23}$$

where $\chi:=\psi+\pi/3$, and a prime denotes differentiation with respect to r. The corresponding Euler-Lagrange equation reads as

$$(r\chi')'=\frac{2\sin 2\chi}{r}. \tag{24}$$

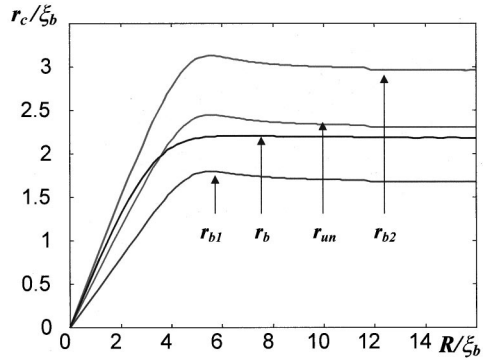

FIG. 3. The influence of confinement on the characteristic lengths r_c for the PR structures. For the PR_+ solution, r_c is either r_{b1}, r_{un}, or r_{b2}, while for the PR_- solution it is just r_b.

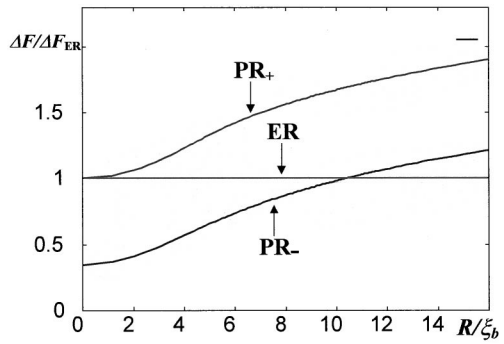

FIG. 4. The excess free energy ΔF for the ER, PR_-, and PR_+ structures normalized to the excess free energy ΔF_{ER} for the ER structure, for different values of R/ξ_b.

After multiplying both sides of Eq. (24) by $r\chi'$ we arrive at a first integral in the form

$$\frac{1}{4}(r\chi')^2=c+\sin^2\chi, \tag{25}$$

where c is an integration constant. Inserting this expression for χ' into Eq. (23) and requiring $\Delta F_{\mathrm{PR}}<\infty$, one obtains $c=0$. A further integration of Eq. (25), subject to the boundary conditions $\psi(1)=2\pi/3$ or $\psi(1)=-\pi/3$, corresponding to the PR_+ or the PR_- solution, respectively, leads to

$$\psi_{\mathrm{PR}+}(r)=\arccos\left(\frac{3r^4-1}{3r^4+1}\right)-\frac{\pi}{3},$$
$$\psi_{\mathrm{PR}-}(r)=\arccos\left(\frac{3-r^4}{3+r^4}\right)-\frac{\pi}{3}, \tag{26}$$

for which $\Delta F_{\mathrm{PR}_+}=8\pi h$ and $\Delta F_{\mathrm{PR}_-}=(8\pi/3)h$ in dimensionless units.

The excess free energies for the ER and the PR solutions are plotted in Fig. 4 as functions of R/ξ_b. One sees that the PR_+ solution is always the most energetic among them. There is a critical value of the ratio R/ξ_b, close to 10.7, marking a transition [31] between the ER and the PR_- solution: below this value the former stores more energy than the latter. It is known from [32] that this transition has indeed a more complex structure: when the ER solution loses stability, there is a range of values for R/ξ_b where the least energetic solution is *planar polar with line defects* [33] (PPLD), that is, a solution with two biaxial *escapes* along the axis of the cylinder, resembling the uniaxial disclination with strength $\frac{1}{2}$. The PPLD solution breaks the symmetry presumed in our parametrization, and so it escapes our model, which instead captures the transition to the PR_- solution, actually prevailing over the PPLD solution for R/ξ_b sufficiently small. Henceforth we take $R/\xi_b\gg 10$, so that the ER solution is the absolute minimizer of the free-energy functional.

To find out in which regime the Lyuksyutov constraint is acceptable, we compare the biaxial PR_- solution to the uniaxial PR_u solution, which requires melting at the cylinder axis. To determine the PR_u solution, we set $\boldsymbol{n}=\boldsymbol{e}_r$ and allow

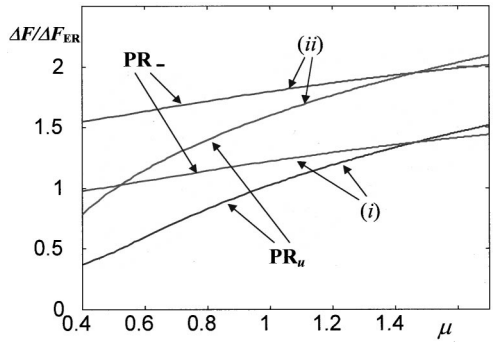

FIG. 5. The excess free energy ΔF for both the PR_- and the PR_u structures normalized to the excess free energy ΔF_{ER} for the ER structure, for different values of the ratio $\mu(\tau) \coloneqq \xi_b(\tau)/\xi(\tau)$. (i) $(R/\xi_b)^2 = 135$, (ii) $(R/\xi_b)^2 = 1350$.

for spatial variations of s in Eq. (3): it is easily shown that in dimensionless units the free energy is then expressed by

$$F_{\mathrm{PR}_u} = \frac{4\pi h}{3} \int_0^1 r\, dr \left(\frac{1}{\xi_n^2} (\tau s^2 - 2s^3 + s^4) + s'^2 + \frac{3s^2}{r^2} \right). \tag{27}$$

The corresponding Euler-Lagrange equation is

$$s'' + \frac{s'}{r} - \frac{3s}{r^2} - \frac{1}{\xi_n^2} (\tau s - 3s^2 + 2s^3) = 0. \tag{28}$$

Figure 5 shows the excess free energy of both the PR_- and the PR_u solution as a function of the ratio $\mu(\tau) \coloneqq \xi_b(\tau)/\xi(\tau) = \sqrt{2}\sqrt{-4\tau + \frac{9}{2} + \frac{3}{2}\sqrt{9-8\tau}}/3\sqrt{3+\sqrt{9-8\tau}}$ between the nematic biaxial and uniaxial correlation lengths (see Appendix). The ''deep nematic'' phase corresponds to the regime where $\mu(\tau) \gg 1$. Just below the *I-N* phase transition, for which $\mu(1) = \frac{1}{3}$, the isotropic solution is preferred. There exists a critical temperature below which the crossover to the PR_- solution (obtained within the Lyuksyutov constraint) takes place. In reality, the value of $\mathrm{tr}\,\mathbf{Q}^2$ drops at the defect core of the PR_- solution [17,18], so pushing the critical temperature towards higher values.

B. Point defects

Here we focus on the biaxial structure of point defects with strength $|M| = 1$, where $\mathbf{Q}$ also depends on the z coordinate. The free energy of the ER solution is invariant under the transformation that reverses the sign of φ_{ER} in Eq. (22). Thus, domains with opposite ER structures are equally likely to arise in an infinitely long cylinder. Wherever two such domains join together, a point defect with topological charge ± 1 appears on the cylinder axis [29,34]. The resulting structure, which is often referred to as ERPD (*escaped radial with point defects*), is metastable and tends to relax towards the topologically equivalent ER structure. An ERPD structure is generally produced on cooling the liquid crystal from its isotropic phase. Each cross section through a defect exhibits a distortion resembling a PR solution, since φ has opposite signs on the two sides of the section, and so must vanish on it. Thus, this section plays the role of a domain wall. Only the PR_+ solution can be accommodated in it, because, unlike

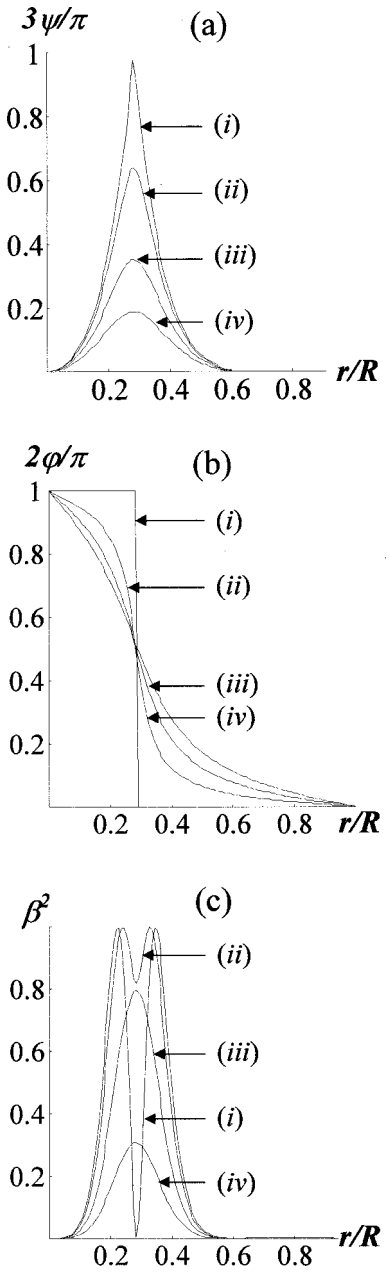

FIG. 6. The graphs of the functions (a) $\psi = \psi(r,z)$, (b) $\varphi = \varphi(r,z)$, and (c) $\beta^2 = \beta^2(r,z)$ for $(R/\xi_b)^2 = 135$, and different values of z: (i) $z = 0$, (ii) $z = \Delta z$, (iii) $z = 2\Delta z$, (iv) $z = 3\Delta z$, where $\Delta z/R = 0.05$. The center of the defect core is at $(r,z) = (0,0)$. The graphs for $z = 0$ in both (a) and (b) reflect the transformation $\{\varphi, \psi\} \to \{\varphi + \pi/2, 2\pi/3 - \psi\}$ for $r < r_{un}$ described in the text.

the PR_- solution, on the cylinder axis it matches both ER domains, which are uniaxial with positive order parameter. It is remarkable that the PR_+ solution, which would never be energetically preferred in the absence of point defects, is indeed relevant to their biaxial structure.

In this study we restrict attention to a single defect of either sign: this effectively amounts to assuming that the distance between two adjacent defects is larger than $2R$, so that their mutual attraction becomes negligible [34]. Within our model the equilibrium biaxial structure of a defect is described by the functions $\varphi = \varphi(r,z)$ and $\psi = \psi(r,z)$: they are represented in Figs. 6, 7 together with the degree of bi-

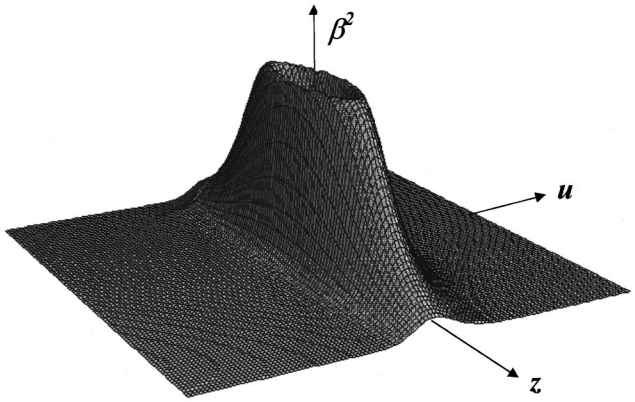

FIG. 7. Two-dimensional plot of β^2 for $R/\xi_b=100$ in the variables $u:=\ln r$ (for $r\geqslant 10^{-3}$) and z. It clearly indicates the cross section of the torus exhibiting a maximal degree of biaxiality.

axiality β^2. The plane at $z=0$ exhibits a structure similar to the one shown in Fig. 2(a), where the nematic state at $r=0$ is described by the pair $\{\varphi,\psi\}=\{0,2\pi/3\}$. On the other hand, just above this plane, but still at $r=0$, the ER structure prescribes the pair $\{\pi/2,0\}$, which by the transformation in Eq. (11) corresponds to the same state. This discontinuity would, however, cause a divergence in the free-energy functional, because it also involves ψ. In our calculations we avoided such a divergence by expressing both the fields φ and ψ and their gradients in the Euler-Lagrange equations through one and the same representation. We privileged the ''perspective'' of the ER solution, and so at $z=0$ we switched from the pair $\{\varphi,\psi\}$ for $r\geqslant r_{un}$ to the pair $\{\varphi+\pi/2,2\pi/3-\psi\}$ for $r<r_{un}$, with r_{un} the point where $\psi=\pi/3$: as in [35], the discontinuity in φ at this point does not make the free-energy functional infinite. The value of φ at $r=r_{un}$ remains arbitrary, reflecting the degeneracy of the eigenvalues of **Q** in the (r,z) plane.

The resulting structure is characterized by the following qualitative features: some are already evident from Figs. 6(c), 7, which show the graph of the function $\beta^2=\beta^2(r,z)$. The symmetry plane at $z=0$ exhibits a *uniaxial ring* with radius $r=r_{un}$ surrounded by biaxial zones with maximal biaxiality at the rings $r=r_{b1}$ and $r=r_{b2}$, as in the PR_+ solution studied above: $\beta^2(r_{b1},0)=\beta^2(r_{b2},0)=1$ with $0<r_{b1}<r_{un}<r_{b2}$, though these values of r are different from those for the genuine PR_+ solution. Just above (or below) $z=0$ the uniaxial ring disappears. Farther away from this plane, both radia r_{b1} and r_{b2} survive, but they vary with z: they approach each other, and eventually merge at $z=\pm z_{b1}$. For $|z|>z_{b1}$ the function β^2 never reaches 1, and it exhibits a single maximum at $r=r_b(z)$, which monotonically decreases with z. The value of $\beta^2(r_b(z),z)$ drops to $\frac{1}{2}$ at $z=\pm z_{b2}$.

In other words, the uniaxial ring with negative order parameter lying in the symmetry plane is surrounded by a *biaxial torus*, where the degree of biaxiality attains its maximum. For R large enough (''saturated'' regime), the torus cross section is circular with radius $r_t\approx 0.8\xi_b$, as shown in Fig. 8(a). In this regime $r_{b1}\approx 4.2\xi_b$, $r_{un}\approx 5.0\xi_b$, $r_{b2}\approx 5.8\xi_b$, $z_{b1}\approx 0.8\xi_b$, $z_{b2}\approx 1.6\xi_b$. For smaller values of R the torus cross section becomes prolate along the z direction. The way the above characteristic lengths depend on the confinement resembles the one obtained for line defects. Some

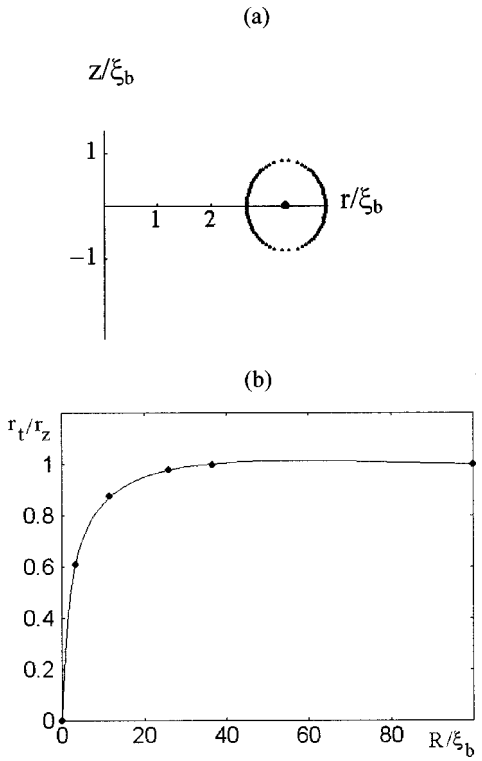

FIG. 8. (a) The cross section of the biaxial torus for $R/\xi_b=11.5$. (b) Influence of the confinement on the aspect ratio of the cross section. The torus width is $2r_t$, while its thickness is $2r_z$. Circles mark calculated points.

preliminary results are shown in Fig. 8(b). We plan to present a detailed study focused on the confining effect of the geometry on the biaxial torus elsewhere.

IV. CONCLUSIONS

The main topic of this contribution is the detailed biaxial structure of nematic line and point defects with strength $|M|=1$ in a cylindrical cavity enforcing homeotropic anchoring. We mainly built on the work by Lavrentovich and co-workers [12,36], Penzenstadler and Trebin [9], Gartland and co-workers [17–19], and Rosso and Virga [16].

We limited attention to the nematic low temperature regime, where a uniaxial liquid crystal responds to distortions by entering biaxial states, rather than melting. We treated only structures with no twist deformation exhibiting cylindrical symmetry. Twisted structures might appear for relatively low values of the twist Frank elastic constant relative to the bend and splay constants [8].

Within this framework we obtained two qualitatively different line defect core structures, referred to as PR_- and PR_+, that basically differ by the sign of the uniaxial order parameter s at the very defect core ($s<0$ in PR_-, and $s>0$ in PR_+). Our results confirm calculations of Sigillo *et al.* [23] based on a molecular approach. In the PR_- structure the line defect is surrounded by a cylinder with radius r_b exhibiting maximal degree of biaxiality. The PR_+ structure, which is more energetic, can be characterized by three coaxial cylinders with radia $r_{b1}<r_{un}<r_{b2}$ displaying, in the order, maximal biaxiality (r_{b1}, r_{b2}), and negative uniaxial ordering in the azimuthal direction (r_{un}). For equal Frank

elastic constants, $r_{b1}\approx 1.7\xi_b$, $r_{un}\approx r_b\approx 2.3\xi_b$, $r_{b2}\approx 3.7\xi_b$ in the regime $R>R_{\rm sat}\approx 5.5\xi_b$, where for typical liquid crystals $\xi_b\approx 10$ nm. Below this regime, confinement effects become significant, pushing characteristic radia towards zero, roughly linearly with R. Note that a homeotropic anchoring with strength W prevails only if $RW/K>1$, where K is a typical nematic Frank elastic constant. For $K\approx 5\times 10^{12}$ J/m and $R\approx R_{\rm sat}\approx 55$ nm, this requires $W>10^{-4}$ J/m^2 for finite size effects to be observed. In addition, the radius must be small enough ($R<4.4\xi_b\approx 45$ nm) for a PR_- core structure to correspond to the absolute minimizer. For typical liquid crystals these limits are rather hard to reach experimentally. It is also to be noted that in the limit for small values of R the validity of the Lyuksyutov constraint is questionable, as is the validity of the elastic approach. Thus, in this regime the results are more of an academic interest.

We explored in detail the biaxial structure of a point defect displaying cylindrical symmetry. Recent results [9,16,17] have shown that this structure is in most cases stable relative to the uniaxial solution. The center of the core is uniaxial along the symmetry axis, with positive order parameter; it is surrounded by a uniaxial ring with negative degree of order and radius r_{un}. The azimuthal plane through the center of the defect has the PR_+ structure typical of a line defect: this structure can thus be characterized by the radia r_{un}, r_{b1}, and r_{b2}, which are, however, approximately twice as large as for the line defect. The ring with $r=r_{un}$ is in the center of the torus displaying maximal biaxiality. In the saturated regime ($R>10\xi_b$) the torus cross section is circular with diameter $2r_t=r_{b2}-r_{b1}$. For equal elastic nematic constants, we obtained $r_{b1}\approx 4.2\xi_b$, $r_{un}\approx 5.0\xi_b$, $r_{b2}\approx 5.8\xi_b$. The position of the uniaxial ring is similar to the one retraceable in Gartland's pioneering simulations [37]. Below the saturated regime the torus cross section takes a shape prolated in the direction of the cylinder axis.

Our preliminary results indicate that in the limit $R/\xi_b\rightarrow\infty$ the core structure of point defects is exactly the same for both spherical and cylindrical confinements. This suggests that the core structure does not depend on the far director field, if the confining cavity is large enough compared to ξ_b. We will focus elsewhere on this universal feature [38].

ACKNOWLEDGMENTS

We thank both E.C. Gartland and A.M. Sonnet for stimulating discussions and comments. This work was supported by the Ministry of Science and Technology of Slovenia (Grant No. Y1-0595, Y2-7609) and the European Community (INCO Copernicus Project IC15-CT96-0744).

APPENDIX: CORRELATION LENGTHS

To obtain estimates for both the uniaxial and biaxial correlation lengths, we express the tensor **Q** in the Cartesian coordinate system with $\{\boldsymbol{e}_1,\boldsymbol{e}_2,\boldsymbol{e}_3\}$: $\boldsymbol{e}_1$ is in the direction of the x axis, along which variations in space are only allowed. The corresponding dimensionless free-energy density is

$$f=\frac{2}{3}\left[\frac{1}{\xi_n^2}(\tau s^2-2s^3\cos 3\psi+s^4)+s^2\left(\frac{d\psi}{dx}\right)^2+\left(\frac{ds}{dx}\right)^2\right]. \tag{A1}$$

We first take the uniaxial case (i.e., $\psi=0$), and locally (at $x=0$) we perturb the order parameter by Δs_0 from its equilibrium value $s(\tau)=s_{\rm eq}$, where $s(\tau)=0$ for $\tau>1$ and $s(\tau)=(3+\sqrt{9-8\tau})/4$ for $\tau\leqslant 1$. We let $s=s_{\rm eq}+\Delta s(x)$ and expand Eq. (A1) about equilibrium, up to the second order in Δs. The solution to the corresponding Euler-Lagrange equation reads as $\Delta s=\Delta s_0 e^{-x/\xi(\tau)}$, where $\xi(\tau)$ is the *nematic correlation length* at the reduced temperature τ:

$$\xi(\tau)=\begin{cases}\dfrac{\xi_n}{\sqrt{\tau}} & \text{for } \tau>1 \qquad (A2)\\[2ex] \xi_n\dfrac{\sqrt{2}}{\sqrt{-4\tau+\dfrac{9}{2}+\dfrac{3}{2}\sqrt{9-8\tau}}} & \text{for } \tau\leqslant 1. \qquad (A3)\end{cases}$$

The quantity ξ_n defines the value of the correlation length at the I-N phase transition, i.e., $\xi_n=\xi(1)$.

We next limit attention to the nematic phase (i.e., $\tau<1$), set $s(x)=s_{\rm eq}$, and perturb locally ψ from its equilibrium value ($\psi=0$). The same approximation described above now leads to defining the biaxial correlation length as

$$\xi_b:=\frac{\xi_n}{3\sqrt{s_{\rm eq}}}. \tag{A4}$$

Taking into account that $24A(T_{IN}-T_*)C/B^2=1$ and that here s is measured in terms of $s_{\rm eq}(T_{IN})$, we then easily retrace the expressions in Eqs. (12) and (13).

[1] N. D. Mermin, Rev. Mod. Phys. **51**, 591 (1976).
[2] O. D. Lavrentovich, Liq. Cryst. **24**, 117 (1998), and references therein.
[3] M. V. Kurik and O. D. Lavrentovich, Usp. Fiz. Nauk **154**, 381 (1988) [Sov. Phys. Usp. **31**, 196 (1988)], and references therein.
[4] M. Kleman, *Points, Lines and Walls* (Wiley, Chichester, 1983).
[5] P. G. de Gennes, Solid State Commun. **10**, 753 (1972).
[6] D. N. Spergel and N. G. Turok, Sci. Am. (Int. Ed.) **3**, 36 (1992).
[7] H. R. Trebin, Liq. Cryst. **24**, 127 (1998), and references therein.
[8] P. G. de Gennes and J. Prost, *The Physics of Liquid Crystals* (Oxford University Press, Oxford, 1993).
[9] E. Penzenstadler and H. R. Trebin, J. Phys. (France) **50**, 1025 (1989).
[10] E. M. Terentjev, Phys. Rev. E **51**, 1330 (1995).

[11] O. D. Lavrentovich and E. M. Terentjev, Zh. Éksp. Teor. Fiz. **91**, 2084 (1986) [Sov. Phys. JETP **64**, 1237 (1986)].
[12] O. D. Lavrentovich, T. Ishikawa, and E. M. Terentjev, Mol. Cryst. Liq. Cryst. Sci. Technol., Sect. A **299**, 301 (1997).
[13] C. Chiccoli, P. Pasini, F. Semeria, T. J. Sluckin, and C. Zannoni, J. Phys. II **5**, 427 (1995).
[14] N. Schopol and T. J. Sluckin, J. Phys. (France) **49**, 1097 (1988).
[15] F. Greco and G. Marrucci, Mol. Cryst. Liq. Cryst. Sci. Technol., Sect. A **210**, 129 (1992).
[16] R. Rosso and E. G. Virga, J. Phys. A **29**, 4247 (1996).
[17] E. C. Gartland and S. Mkaddem (unpublished).
[18] E. C.Gartland (unpublished).
[19] E. C. Gartland, P. Palffy-Muhoray, and R. S. Varga, Mol. Cryst. Liq. Cryst. **199**, 429 (1991).
[20] S. Kralj, S. Žumer, and D. W. Allender, Phys. Rev. A **43**, 2943 (1991).
[21] A. Sonnet, A. Kilian, and S. Hess, Phys. Rev. E **52**, 718 (1995).
[22] N. Schopohl and T. J. Sluckin, Phys. Rev. Lett. **59**, 2582 (1987).
[23] I. Sigillo, F. Greco, and G. Marrucci, Liq. Cryst. **24**, 419 (1998).
[24] P. Biscari and E. G. Virga, Int. J. Non-Linear Mechanics **32**, 337 (1997).
[25] P. Kaiser, W. Wiese, and S. Hess, J. Non-Equilib. Thermodyn. **17**, 153 (1992).
[26] A. L. Alexe Ionescu, R. Barberi, G. Barbero, and M. Giocondo, Phys. Lett. A **190**, 109 (1994).
[27] I. F. Lyuksyutov, Zh. Éksp. Teor. Fiz. **75**, 358 (1978) [Sov. Phys. JETP **48**, 178 (1987)].
[28] W. H. Press, B. P. Flannery, S. A. Teukolsky, and W. T. Vetterling, *Numerical Recepies* (Cambridge University Press, Cambridge, England, 1986).
[29] D. W. Allender, G. P. Crawford, and J. W. Doane, Phys. Rev. Lett. **67**, 1442 (1991).
[30] C. Williams, P. Pieranski, and P. E. Cladis, Phys. Rev. Lett. **29**, 90 (1972).
[31] P. Ziherl and S. Žumer, Liq. Cryst. **21**, 871 (1996).
[32] A. Kilian and A. Sonnet, Phys. Rev. E **52**, 2702 (1995).
[33] S. Kralj and S. Žumer, Phys. Rev. E **51**, 366 (1995).
[34] G. Guidone Peroli and E. G. Virga, Phys. Rev. E **54**, 5235 (1996).
[35] L. Ambrosio and E. G. Virga, Arch. Ration. Mech. Anal. **114**, 335 (1991).
[36] O. D. Lavrentovich and E. M. Terentjev (unpublished).
[37] E. C. Gartland (unpublished).
[38] E. G. Virga and S. Kralj (unpublished).